A comparative study of the synthesis of nanocrystalline Yttrium Aluminium Garnet using sol-gel and co-precipitation methods

Ramanujam, Prabhu; Vaidhyanathan, Bala; Binner, Jon; Anshuman, Aashu; Spacie, Chris

DOI:
10.1016/j.ceramint.2013.08.075

Document Version
Peer reviewed version

Citation for published version (Harvard):
Ramanujam, P, Vaidhyanathan, B, Binner, J, Anshuman, A & Spacie, C 2014, 'A comparative study of the synthesis of nanocrystalline Yttrium Aluminium Garnet using sol-gel and co-precipitation methods', *Ceramics International*, vol. 40, no. 3, pp. 4179-4186. https://doi.org/10.1016/j.ceramint.2013.08.075

Journal of Nanoparticle Research

A comparative study of the synthesis of nanocrystalline YAG using sol-gel and co-precipitation methods

--Manuscript Draft--

Manuscript Number:	
Full Title:	A comparative study of the synthesis of nanocrystalline YAG using sol-gel and co-precipitation methods
Article Type:	Original research
Keywords:	Keywords: Yttrium aluminium garnet, sol-gel, co-precipitation, nanoparticles
Corresponding Author:	Prabhu Ramanujam, M.Sc., M.Tech Loughborough University Loughborough, Lecistershire UNITED KINGDOM
Corresponding Author Secondary Information:	
Corresponding Author's Institution:	Loughborough University
Corresponding Author's Secondary Institution:	
First Author:	Prabhu Ramanujam, M.Sc., M.Tech
First Author Secondary Information:	
Order of Authors:	Prabhu Ramanujam, M.Sc., M.Tech
	Bala Vaidhyanathan
	Jon Binner
	Aashu Anshuman
	Chris Spacie
Order of Authors Secondary Information:	
Abstract:	Abstract: Nanocrystalline yttrium aluminium garnet (nYAG) powder has been synthesized via sol-gel and co-precipitation methods using nitrate precursors. Thermal evolution and crystallisation kinetics of both the methods were investigated. The optimised calcination condition for the formation of nYAG was also examined. It was found that a complete transformation to nYAG was observed at 925°C/2h and 1000°C/1h for the co-precipitation and sol-gel samples respectively. An intermediate YAlO3 phase was formed at 900°C in all powders regardless of the synthesis methods. The powder morphologies obtained from TEM revealed very similar particle sizes for the two routes (20-30 nm); whilst the extent of agglomeration was higher for the sol-gel method. It was also observed that by controlling the pH in a narrow range, maintaining the precipitate processing temperature and dehydrating excess OH- ions in the precipitates using an n-butanol treatment, the extent of agglomeration was further reduced in the co-precipitated nYAG powder.
Suggested Reviewers:	Palmero Paola Polytechnic University of Turin paola.palmero@polito.it He worked on co-precipitation synthesis of nanocrystalline YAG
	Sanjay Mathur University of Cologne sanjay.mathur@uni-koeln.de He worked on sol-gel synthesis of nano materials including YAG. He has lot of experience in YAG nano particles.

List of authors and Affiliations

1) Mr Prabhu Ramanujam,

PhD student,

S208, Department of Materials, Loughborough University,

Loughborough, Leicestershire, LE11 3TU, UK

Mobile: 0044 07505964261

Email: p.ramanujam2.lboro.ac.uk

2) Dr. Bala Vaidhyanathan (Corresponding author),

Department of Materials, Loughborough University,

Loughborough, Leicestershire, LE11 3TU, UK

Tel: +44-01509-223152

Fax: 0044 01509 223949

Email: B.Vaidhyanathan@lboro.ac.uk

3) Professor Jon Binner,

Department of Materials, Loughborough University,

Loughborough, Leicestershire, LE11 3TU, UK

Tel: +44-1509-223330

Fax: +44-1509-223949

Email: j.binner@lboro.ac.uk

4) Mr Aashu Anshuman

Department of Ceramic Engineering,

IIT(BHU), Varanasi, India

5) Dr. Chris Spacie

Morgan Advanced Materials & Technology, Swansea, UK

A comparative study of the synthesis of nanocrystalline YAG using sol-gel and co-precipitation methods

Prabhu Ramanujam[a#], Bala Vaidhyanathan[a], Jon Binner[a], Aashu Anshuman[b] and Chris Spacie[c]

[a]Department of Materials, Loughborough University, Loughborough, UK

[b]Department of Ceramic Engineering, IIT(BHU), Varanasi, India

[c]Morgan Advanced Materials & Technology, Swansea, UK

[#]*Author for correspondence, Email: b.vaidhyanathan@lboro.ac.uk*

1 Introduction

Ceramic powder processing within the Y_2O_3-Al_2O_3 system has largely been intended for optical and structural applications. In this system, three stable yttrium aluminates exist with different polymorphs, perovskite-based orthorhombic $YAlO_3$ (YAP), monoclinic $Y_4Al_2O_9$ (YAM) and garnet $Y_3A1_5O_{12}$ (YAG) (Abell et al. 1974). The latter is rich in Al_2O_3 and crystallises with cubic symmetry. It does not exhibit any birefringence effects at the grain boundaries and hence results in high in-line transparency. A hexagonal $YAlO_3$ (YAH) has also been identified as an intermediate metastable phase during the processing of YAG (Tanner et al. 2003).

The choice of powder synthesis route has a significant effect on powder characteristics such as size, shape, distribution and the extent of agglomeration, each of which greatly influences the microstructural homogeneity of the resulting ceramics (Akio Ikesue, Yan Lin Aung,Takunori Taira, Tomosumi Kamimura, Kunio Yoshida, Gary L. Messing 2006). Each factor has the potential to introduce an adverse effect on densification and microstructure of the ceramics. The presence of particle agglomeration, for example, is a well-known source of inhomogeneity, and hence defects, in the final microstructure of ceramic components (Lange 1989). Therefore, efforts have been made to produce high quality ceramic powders by a range of synthesis routes.

The conventional method for preparing YAG involves mixing Y_2O_3 and Al_2O_3 in a 3:5 molar ratio and then calcining at 1600°C for prolonged times together with repeated grinding (Li et al. 2007). Wet chemical routes such as sol-gel (Gowda 1986), co-precipitation (Li et al. 2004), solvo-thermal (Wang et al. 2006) and combustion (Devi et al. 2002, Ramanathan et al. 2003) routes are promising methods for synthesising high purity single phase YAG at relatively low temperatures, though there are some disadvantages. Solvo-thermal synthesis, for example, requires the use of an autoclave and pressures of about 70–175 MPa, whilst combustion synthesized powders result in chemical inhomogeneities and particle agglomeration due to the intense local

heating. In contrast, sol-gel and co-precipitation synthesis can be low cost and are more likely to yield homogenous YAG powders. The use of alkoxide precursors (Veith et al. 1999) leads to crystallisation from 700 - 1000°C and the resultant powder consequently exhibits particle sizes of about 60-80 nm with heavy agglomeration. In contrast, nitrate (Hou et al. 2009) and chloride (Tachiwaki et al. 2001) precursors lead to crystallisation at about 950°C, although chlorine ions are more difficult to rinse from the hydroxide precipitate, even with washing. The presence of chlorine ions results in hard agglomerates in the nanopowder (Wang et al. 2010) and hence has negative effects on the mechanical properties of the subsequent ceramic. To reduce the level of agglomeration, several complexing and precipitating agents have been examined for both sol-gel and co-precipitation methods using nitrate precursors. Nanocrystalline YAG was synthesised using citric acid as a chelating ligand in sol-gel method, (Vaqueiro and Arturo Lopez-quintela 1998). This resulted in rod shaped particle morphology with particle sizes in the range of 20-70 nm and significant agglomeration was still observed. Recently, Yang (2010) optimised the solvent concentration and calcination conditions to achieve nano YAG with soft agglomerates using a sol-gel method. This work also confirmed that the molar concentration ratio of the Y^{3+} and Al^{3+} ions in the precursor solution has a significant effect on particle size. Wang (2000) also studied the effect of different concentrations of precursor solution for the co-precipitation synthesis of YAG nano powder. They achieved 20-30 nm particles using a precursor solution ratio of <1 and calcination for 2 hours at 900°C. The uses of different precipitants (Li et al. 2000) and pH conditions (Apte et al. 1992, Palmero et al. 2005) have also been studied; these are also considered to be very important factors governing particle morphology with the co-precipitation method. Li (2000) studied the effect of precipitants using ammonium hydroxide and ammonium hydrogen carbonate (AHC) with a precursor solution ratio of about 1.5 at pH 9. Their comparative study suggests that the YAG powder synthesized using AHC resulted in less agglomeration with crystallite size of about 52 nm. However, neither the precursor concentration, nor the control over the pH was optimized. Apte and Vrolijk (1992, 1990) investigated the best pH range for the precipitating YAG using ammonium hydroxide was investigated and suggested that it was pH 7 – 9. Palmero (2005) investigated the influence of calcination temperature on the phase evaluation of YAG from 800 - 1100°C, but omitted 950 and 1000°C/1h, the powders were over calcined at 1100°C and resulted in large particles with heavy agglomeration.

These results suggest that identification of the most suitable processing conditions is still required for the production of fine, nanocrystalline YAG displaying little agglomeration. In the present work, the syntheses of nano YAG by sol-gel and co-precipitation methods are compared with a view to optimising the processing conditions and determining the formation mechanisms.

2 Experimental

2.1 Materials

99.9% $Y(NO_3)_3.6H_2O$ and $\geqslant$ 98% $Al(NO_3)_3.9H_2O$, both from Sigma Aldrich, Dorset, UK were used as the source of Y^{3+} and Al^{3+} ions. 99.9% citric acid, also from Sigma Aldrich, was used as the complexing agent for the sol-gel synthesis. 35% ammonium hydroxide and 99% *n*-butanol, both from Fisher Chemicals, Loughborough, UK were used as the precipitating agent for the cations and for dehydrating them in the co-precipitation method, respectively.

2.2 Synthesis

2.2.1 Sol-gel

A solution containing the stoichiometric ratio of 3:5 (Y:Al) was prepared by mixing calculated amounts of 0.6M $Y(NO_3)_3.6H_2O$ and 1M $Al(NO_3)_3.9H_2O$ aqueous solutions in 1M citric acid solution. The schematic representation of the sol-gel process is shown in figure 1a. Homogenous mixing was achieved in a round bottom (RB) flask equipped with a magnetic stirrer and a refluxing condenser. The reaction flask was immersed in a thermostatic oil bath and refluxed at 90±10°C for 24 hours. During mixing, the transparent precursor sol underwent substitution and polymerization reactions to form a transparent gel, which was then dried in an oven at 100°C for 24 hours. The fluffy mass obtained after drying was subsequently ground using an agate pestle and mortar for further characterisation.

2.2.2 Co-precipitation

The reverse strike co-precipitation method used involved mixing the same 0.6M $Y(NO_3)_3.6H_2O$ and 1M $Al(NO_3)_3.9H_2O$ aqueous solutions for 2 hours. The schematic representation of the co-precipitation process is shown in figure 1b. This precursor solution was placed in a burette and added drop-wise to 200 ml of the aqueous NH_4OH precipitant solution whilst simultaneously stirring and maintaining the pH at 8.20 ± 0.05. The first few drops of the precursor solution were found to decrease the pH rapidly to 4; therefore excess ammonia solution of 5M concentration was added concurrently to maintain the pH. Continuous monitoring of the pH allowed it to be controlled to ± 0.05 pH units. The resultant precipitate was filtered, washed three times with dilute ammonia solution of pH 8.2 to remove nitrate residues, and then the filtered precipitate was dispersed

with 20 ml of *n*-butanol using ultrasound for two minutes. The dispersed precipitate was dried at 100°C for 24 hours and ground using the pestle and mortar.

The precursor powders from the sol-gel (SG-nYAG) and co-precipitation (CP-nYAG) routes were then calcined for 1 or 2 h in a silica crucible at temperatures in the range 900 - 1000°C in an air atmosphere, using a heating and cooling rate of 10°C/min.

2.3 Powder characterisation

Thermal analysis of the dried SG-nYAG and CP-nYAG precursor powders was performed using simultaneous TGA/DSC (SDT 2960, TA Instruments, USA). The precursors were weighed to 25 mg and placed into an alumina sample pan with a clean, empty alumina pan used as a reference. All TGA/DSC traces were recorded between 25°C and 1000°C at a ramp rate of 10°C min^{-1} under flowing air. Fourier transform-infrared spectroscopy (FT-IR 8400S, Shimadzu, Maryland, USA) was used to identify structural features in the precursors and heat-treated powders. Transmission FTIR was carried out over the wavenumber range of 4000 – 400 cm^{-1}. All samples for FTIR measurement were well mixed with KBr in a weight ratio of 1:20 and then pressed into translucent pellets. The crystalline structure of the calcined nano powders was characterised using X-ray diffraction (Bruker D8, Bruker AXS GmbH, Karlsruhe, Germany, fitted with a quarter-circle Eulerian cradle). All the powder samples were analysed at a step size of 0.02° whilst the XRD patterns were recorded from 20° to 90°. TEM, (JEOL JEM 2000FX, JEOL Ltd. Tokyo, Japan) was used to study the particle size of the powders. The samples for TEM were prepared by dispersing the powders in an alcohol medium using ultrasound and then a drop of the suspension was deposited on a carbon film, from Agar Scientific, Stansted, UK. The TEM samples were dried in a laboratory oven at 60°C for 15 minutes and loaded into a single tilt holder. The TEM was operated at 200 kV and the images were obtained at different magnifications.

3 Results and Discussion

3.1 TGA/DSC

The thermal analysis curves for the dried SG-nYAG and CP-nYAG precursor powders are shown in figures 2a and 2b. The curves show 45 wt% and 35 wt% total weight loss for the dried SG-nYAG and CP-nYAG precursor powders respectively. The difference in the weight loss for the co-precipitation route is due the removal of ~10% of the organics in the precipitates during filtering and washing before the heat treatment. Nevertheless,

these results match with the conversion yield of the YAG powders, 19.6 wt %, after thermal decomposition of the precursors from both the methods. The substantial weight loss from 100–600°C is associated with the decomposition of the organics in the precursors. The difference in total weight loss between the powders and the crystallisation kinetics are described with the endotherms and exotherms provided by the DSC analyses.

For the SG-nYAG powder, figure 2a, an endothermic peak near 390°C corresponds to the decomposition of NO_3^- and CO_2(Lu et al. 2002)due to the redox reaction between them, where citrate acts as a reductant and the nitrate as an oxidant (Li et al. 2008). The second endothermic peak at 450°C is attributed to the oxidation of free carbon from the incomplete combustion of carboxylate groups in the citric acid (Li et al. 2008). As the temperature exceeded 600°C, the weight loss became insignificant and the transition of the crystalline phase proceeded with the change in heat capacity. An exothermic peak observed near 917°C indicates the onset crystallization temperature, T_c.

The DSC result for the CP-nYAG powder, figure 2b, confirms that the loss of organics during heat treatment is less than for the SG-nYAG powder and the reaction mechanism is simpler. The first endothermic peak near 170°C can be attributed to the removal of butanol; this is due to the substitution of surface hydroxyl groups by the butoxyl groups in the precipitates (Qiu et al. 1995). The small endothermic peaks from 300 - 500°C are due to the decomposition of residual CO_2, NO_2 and NH_4 in the powder. These endotherms explain the difference in weight loss in the TGA curves between the two powders. The excess hydroxyl molecules and NO_3^- ions will be removed during the filtering stage in the co-precipitation process. The exotherm observed near 916°C corresponds to the onset crystallisation temperature for YAG (similar to the SG-nYAG powder).

3.2 FT-IR analysis

Further investigation of the crystalline transition and the decomposition pathways of the two powders were performed using FT-IR spectroscopy. The goal was to obtain an improved understanding of the crystallisation kinetics and the relevant formation mechanisms.

FT-IR spectra from 4000 - 400 cm^{-1} for the two powders after heat treatment at different temperatures are shown in figures 3a and 3b. The broad absorption bands near ~3450 cm^{-1} and ~1630 cm^{-1} in both powders at 100°C are associated with the O-H stretching vibrations of coordinated water molecules and the characteristics of H–O–H bending modes of molecular water (Su et al. 2005, Tanner et al. 2003).

The COOH functional groups, chelating ligands, near ~1729, ~1450 and ~1323 cm^{-1} in the SG-nYAG curve, figure 3a, after drying at 100°C are associated with the carboxyl vibrations of the citric acid. The weak band near ~1729 cm^{-1} coincides with ν(C=O) stretching (Ojamäe et al. 2006), which suggests that not all the carboxyl groups are bonding with the metal cations or free ν(C=O) exists. The other two bands near ~1450 cm^{-1} and ~1323 cm^{-1} are associated with the symmetric ν_s(C=O) and asymmetric ν_{as}(C=O) vibrations(Rajendran and Rao 1994, Xia et al. 2005), which implies that the dissociated carboxylic ions from the citric acid react to form bonds with the Al^{3+} and Y^{3+} ions, forming a coordinative complex structure between the ligands and the metal ions(Motta et al. 2008, Tanner et al. 2003). The nitrate groups were also observed at ~1380 cm^{-1} and ~825 cm^{-1}, which corresponds to ν(NO_2) and ν(NO_3), respectively(Li et al. 2008). After heat treatment at 600°C, the unreacted ν(C=O), ν(NO_3) and δ(CO) scissoring band (~1037 cm^{-1}) disappear and some traces of the ν_{as} and ν_s of C=O, along with ν(NO_2) vibrations, are still present in the SG-nYAG curve. This demonstrates that ν_{as} and ν_s (C=O) and ν(NO_2) were involved in the redox reaction(Li et al. 2008) and also supplements the thermal analysis results for the SG-nYAG powder. After heat treating at 925°C, the new bands near ~783, ~713 and ~680 cm^{-1}, associated with the metal–oxygen vibration characteristics of Al–O, Y–O, and Y–O–Al stretching confirms the formation of the YAG phase[15] and also coincides with the onset crystallisation peak observed from the DSC results. Nevertheless, the ν(NO_2) vibration is still present in the SG-nYAG powder after heat treatment at 1000°C for 1h, which suggest that some traces of nitrate persists, even after calcination with the sol-gel route.

The FT-IR spectra for the as-dried CP-nYAG powder, figure 3b, displayed very few functional groups when compared to the dried SG-nYAG powder. This also confirms the reaction mechanism between the precipitations is simple and most of the organics were removed during the washing process. The bands near ~1460 cm^{-1} and ~1380 cm^{-1} are associated with the vibrations of ν(NH) and ν(NO_2)(Chen et al. 2007), whilst the peak intensities of the H–O–H bending modes (~1630 cm^{-1}) and ν(NO_2) were apparently low and the ν(NO_3) vibrations present in the SG-nYAG (100°C) trace were absent in the equivalent CP-nYAG curve. This could be due to the effect of ammonia washing and the dehydration effect of the *n*-butanol treatment on the precipitates. The intensities of these bands were further reduced in the CP-nYAG curve after heat treatment at 600°C and there was also agreement with the thermal decomposition results. On further heat treatment at 925°C, the triplet bands formed between 800 - 600 cm^{-1} correspond to the vibrations of Al-O, Y-O and Y-O-Al stretching, which coincides with the crystallisation peak of the DSC analysis. Moreover, the ν(NO_2) band present in the SG-nYAG after calcination at 1000°C for 1 hour is absent in the equivalent curve for the CP-nYAG powder, which confirms that the nitrate ions are removed during the co-precipitation synthesis method.

3.3 XRD - YAG formation

Figures 4a and 4b show the phase evolution as a function of temperature and time for the SG-nYAG and CP-nYAG powders respectively. The obtained peaks are compared with the standard JCPDS card no: 33-0040.

After being heat-treated at 900°C for 2 h and 925°C for 1 h, some traces of the metastable hexagonal h-$YAlO_3$ (YAH) phase was observed for both the SG-nYAG and CP-nYAG powders. However, after heat treating at 925°C for 2 h, no detectable YAH phase was observed for the CP-nYAG powder; whilst the SG-nYAG powder still displayed characteristic peaks of the YAH phase. These peaks were still present after 1 h at 950°C, but disappeared after heat treating for 1 h at 1000°C for the SG-nYAG powders. Thus, after heat treatments of 2 h at 925°C (CP-nYAG) and 1 h at 1000°C (SG-nYAG), all the peak positions matched with the standard YAG diffraction reference pattern and no intermediate phases such as YAM or YAP were observed. Only the metastable YAH formed as an intermediate, which subsequently transformed to YAG at elevated temperatures.

3.4 Mechanisms of YAG formation

Possible mechanisms for YAG formation via the sol-gel and co-precipitation routes are proposed based on the analytical evidence obtained from the thermal analysis, FT-IR spectroscopy and XRD of the precursor powders after heat treatment at different temperatures.

3.4.1 Sol-gel mechanism

The mixing of citric acid, $C_3H_4OH\ (COOH)_3$, with deionised water results in partial dissociation of H^+ ions from the chelating ligands (COOH) and protonation of the water, equation 1. The solvation of the metal cations, introduced as metal nitrates is described by equation 2(Brinker and Scherer 1990).

$$C_3H_4OH\ (COOH)^3 + H_2O\ \rightarrow C_3H_4OH\ (COO^-)^3 + H_3O^+ \quad (1)$$

$$Al(NO_3).9H_2O + Y(NO_3).9H_2O + \ H_2O\ \rightarrow\ (OH_2)Al - Y(OH_2)_{aq} + \ HNO_3 \quad (2)$$

$$\begin{pmatrix} (OH_2)Al - Y(OH_2)_{aq} + \ HNO_3 \\ + C_3H_4OH(COO^-)_3 + H_3O^+ \end{pmatrix} \rightarrow \begin{pmatrix} (COO^-)_3\ Al^{3+} - Y^{3+}(COO^-)_3 + HNO_3 \\ + C_3H_4OH + H_2O + H_3O^+ \end{pmatrix} \quad (3)$$

The second step involved adding the solvated precursor solution into the citrate solution to achieve the substitution reaction given in equation 3. A coordinative complex structure was formed between the metal cations and citrate anions (Blosi et al. 2009).

During drying, the precursor sol partially hydrolysed to form a cross-linked polymer chain between the chelating ligands and the metal ions, i.e. it formed a gel that was, in turn, dried to form a porous fluffy mass, which was ground further and then calcined. Equation 4 and 5 show the reactions being followed during calcination:

$$\begin{pmatrix}(COO^-)_3\,Al^{3+}{-}Y^{3+}(COO^-)_3 + HNO_3 \\ +\,C_3H_4OH + H_2O + H_3O^+\end{pmatrix} \xrightarrow{600\,℃} \begin{pmatrix}(COO^-)_3\,Al^{3+} - Y^{3+}(COO^-)_3 \\ +\,NO_2^- + (CO_2)\uparrow\end{pmatrix} \quad (4)$$

$$(COO^-)_3\,Al^{3+}{-}Y^{3+}(COO^-)_3 + NO_2^- \xrightarrow{1000\,℃} Y_3Al_5O_{12} \quad (5)$$

During calcination at 1000°C, the transformation of the $(COO^-)_3Y^{3+}$-$Al^{3+}(COO^-)_3$ network to metal oxygen bonding (M-O-M) took place and complete crystallisation was achieved, as supported by the thermal analysis and XRD data. A thermally induced anionic redox reaction (reduction and oxidation) took place between the $(COO^-)_3$ and the NO_2^-, with the citrate acting as a reductant and the nitrate as an oxidant(Li et al. 2008).

3.4.2 Co-precipitation mechanism

The co-precipitation process for YAG requires an accurate control over the pH. This is because of the difference in saturation solubility of the yttrium hydroxide and amphoteric aluminium hydroxide (which can react as both an acid and a base). These are stable at different pH range, i.e. pH 7 - 9 for $Y(OH)_3$ and pH 5 - 9 for $Al(OH)_3$(Pourbaix 1974). If the pH is not maintained between the above specified ranges, then the hydroxides redissolve into M^{3+} ions, M = Y or Al, resulting in a heterogeneous precipitation. Besides the pH control, the particle size of the precipitate was controlled by the concentration of the precipitating species and the nucleation and growth of the precipitates (Townshend and Jackwerth 1989).

In this process, the stoichiometric amounts of yttrium and aluminium nitrate were mixed to obtain an aqueous solution of the metal ions and HNO_3, equation 2. Equation 6 explains the co-precipitation reaction between the solvated precursor solution and the $NH_4OH_{(aq)}$ solution. The presence of nitrate ions in the precursor solution makes it even more critical to sustain the pH for precipitation. Therefore, the concentrated precipitant solution was added concurrently to maintain the pH. In the present work, the concentration ratio of the precursor solution was kept at <1, a narrow pH window (±0.05) was maintained and a precipitation rate of about 4 ml/min was used to control the nucleation and growth of the homogenous precipitates. In addition, a nucleophilic substitution reaction between the precursor solution and the NH_4OH occurred yielding an aqueous ammonium nitrate (NH_4NO_3) and H_2O.

$$Al(NO_3).9H_2O + Y(NO_3).9H_2O + H_2O \rightarrow (OH_2)Al - Y(OH_2)_{aq} + HNO_3 \quad (2)$$

$$(OH_2)Al - Y(OH_2)_{aq} + HNO_3 + NH_4OH_{(aq)} \rightarrow Al(OH)_3 - Y(OH)_3 + NH_4NO_{3_{(aq)}} + H_2O \quad (6)$$

$$Al(OH)_3 - Y(OH)_3 + NH_4NO_{3_{(aq)}} + H_2O \xrightarrow{600\,℃} Y - O - Al \xrightarrow{925\,℃} Y_3Al_5O_{12} \quad (7)$$

Equation 7 describes the possible reaction mechanism during calcination. The metal hydroxides are oxidized to form an amorphous Y-O-Al (M-O-M bonding) network and the atomic diffusion between them transformed to a crystalline YAG phase at 925°C. The overall reaction is accompanied by the thermal decomposition of the volatiles and crystallisation kinetics of the CP-nYAG precursor as obtained from thermal analysis, FT-IR and XRD.

3.5 TEM morphology

Figure 5 shows the TEM images of the SG-nYAG and CP-nYAG powders. It is evident that for both powders the primary particle size is in the range between 20-30 nm and a significant degree of agglomeration occurs for the SG-nYAG powder, figures 5a and 5b. This could be due to the complex networking of metal ions in the gel matrix, which the organics were burned off from the network, and led to a severe agglomeration of the primary particles.

When the results obtained in the present work are compared to the literature, the particle size observed by (Chen et al. 2007, Wang et al. 2000), both using co-precipitation, was in a similar region, 30-60 nm, but their powders displayed a higher degree of agglomeration. One reason for our CP-nYAG particles being a little finer, figures 5c and 5d, might be due to the lower calcination temperature used, whilst the reduced degree of agglomeration might be attributed to three possible effects, (i) controlling the pH with a minimal tolerance, (ii) suitable thermal conditions for precipitation and (iii) dehydrating the hydroxyl ions by the *n*-butanol treatment.

Controlling the pH is considered to be the most important factor during co-precipitation reactions. In this case, the precipitating conditions for Y^{3+} and Al^{3+} ions are different for nitrate precursors; Y^{3+} ions precipitates at pH 8.1 whilst Al^{3+} precipitates at pH 3.5(Apte et al. 1992). To avoid the heterogeneity of the co-precipitation, aqueous solutions of Y^{3+} and Al^{3+} ions were mixed and added drop-wise to the precipitant solution, which was maintained at pH 8.20±0.05 by adding concentrated NH_4OH concurrently. It was observed that when the pH of the precipitant solution increased or decreased by just 0.10, both the homogeneity and the morphology of the precipitates changed, Figure 6.

From Figure 6a, it is clear that whilst the precipitates are approximately spherical, there was a significant variation of their size, which is due to the difference in precipitating conditions of Y^{3+} and Al^{3+} ions. When the pH was maintained at 8.20±0.05, Figure 6b, the hydroxides of the mixed metal cations displayed a stable nanostructure and the precipitates were found to be discrete and to have a uniform size distribution. In contrast, bulk precipitation morphology is displayed in Figure 6c. When the pH was increased to 8.30±0.05, the precipitation reaction surpasses the saturation limit and resulted in agglomeration of the precipitates. This could be due to the excess OH^- ions provided by the NH_4OH solution, which dissolves $Al(OH)_3$ (acts as a Lewis acid) into AlO_2^- ions (Pourbaix 1974) and resulted in heterogeneous precipitation. At the best pH conditions (8.20±0.05) a closer look at the nanostructure of the precipitates reveals the formation of a clear core-shell structure, figure 7, during the co-precipitation process. Similar results were reported by Wang (2000) at pH values of 8 which retard the agglomeration.

The effect of processing temperature is shown in the figure 8. From the results, it is evident that the thermal conditions such as 10±1°C and 20±1°C (figure 8a and 8c) resulted in bulk precipitation, which could result in composition inhomogeneity and particle agglomeration. The precipitates processed between these conditions, 13±3°C (figure 8b), offered a homogenous precipitation. The TEM result suggests that a suitable processing temperature is also appears to be required for obtaining homogenous precipitates.

During the *n*-butanol treatment, the surface hydroxyl groups are replaced by the butoxyl groups and thus form an azeotropic layer (Qiu et al. 1995), which acts as a potential barrier between the particles. Due to the low surface tension of *n*-butanol compared to water, the binding force among the particles decreased whilst drying and so hard agglomeration caused by the capillary forces was avoided. Consequently, depletion of the excess OH^- ions in the precipitates controlled the agglomeration during drying and resulted in soft agglomerates of the dried precipitates.

4 Conclusions

Nanocrystalline YAG powders have been synthesised *via* sol gel and co-precipitation using nitrate precursors. The thermal and phase evolution for the formation of nYAG were investigated using DTA/DSC, FT-IR and XRD techniques. It has been observed that 925°C/2h and 1000°C/1h are the optimum temperatures to calcine nYAG by the co-precipitation and sol-gel methods respectively. From the TEM morphologies, the CP-nYAG route yielded particle sizes of 25-30 nm with less agglomeration when compared to the sol-gel synthesis. The

proposed co-precipitation mechanism suggests that an extremely narrow pH range (8.2±0.05), processing temperature (13±3°C) and the effective dehydration of n-butanol appears to be required for production of a homogeneous nYAG powder.

5 Acknowledgement

The authors would like to thank Morgan Advanced Materials, Swansea, UK, for their financial support. The authors also thank LMCC staff at Loughborough University and colleagues in the Advanced Ceramic Research Group for their kind help and support during this project.

6 List of figures:

7 References

Abell JS, Harris IR, Cockayne B, Lent B (1974) An investigation of phase stability in the Y2O3-Al2O3 system. J Mater Sci 9:527-537

Akio Ikesue, Yan Lin Aung,Takunori Taira, Tomosumi Kamimura, Kunio Yoshida, Gary L. Messing (2006) Progress in Ceramic Lasers. Annu Rev Mater Res 36:397-429

Apte P, Burke H, Pickup H (1992) Synthesis of yttrium aluminum garnet by reverse strike precipitation. Journal of Materials Research 7:706-711

Blosi M, Albonetti S, Dondi M, Costa A, Ardit M, Cruciani G (2009) Sol–gel combustion synthesis of chromium doped yttrium aluminum perovskites. J Sol Gel Sci Technol 50:449-455

Brinker CJ, Scherer GW (1990) The Physics and Chemistry of Sol–Gel Processing, New York

Chen Z, Yang Y, Hu Z, Li J, He S (2007) Synthesis of highly sinterable YAG nanopowders by a modified co-precipitation method. J Alloys Compounds 433:328-331

Devi PS, Lee Y, Margolis J, Parise JB, Sampath S, Herman H, Hanson JC (2002) Comparison of citrate-nitrate gel combustion and precursor plasma spray processes for the synthesis of yttrium aluminum garnet. J Mater Res 17:2846-2851

Gowda G (1986) Synthesis of yttrium aluminates by the sol-gel process. J Mater Sci Lett 5:1029-1032

Hou J, Kumar R, Qu Y, Krsmanovic D (2009) Crystallization kinetics and densification of YAG nanoparticles from various chelating agents. Mater Res Bull 44:1786-1791

Lange FF (1989) Powder Processing Science and Technology for Increased Reliability. J Am Ceram Soc 72:3-15

Li X, Liu H, Wang J, Cui H, Han F, Zhang X, Boughton R (2004) Rapid synthesis of YAG nano-sized powders by a novel method. Materials Letters 58:2377-2380

Li C, Zuo H, Zhang M, Han J, Meng S (2007) Fabrication of transparent YAG ceramics by traditional solid-state-reaction method. Transactions of Nonferrous Metals Society of China 17:148-153

Li J, Pan Y, Qiu F, Wu Y, Guo J (2008) Nanostructured Nd:YAG powders via gel combustion: The influence of citrate-to-nitrate ratio. Ceram Int 34:141-149

Li J, Ikegami T, Lee J, Mori T, Yajima Y (2000) Co-precipitation synthesis and sintering of yttrium aluminum garnet (YAG) powders: the effect of precipitant. Journal of the European Ceramic Society 20:2395-2405

Lu Q, Dong W, Wang H, Wang X (2002) A Novel Way to Synthesize Yttrium Aluminum Garnet from Metal-Inorganic Precursors. J Am Ceram Soc 85:490-492

Motta FV, Marques APA, Escote MT, Melo DMA, Ferreira AG, Longo E, Leite ER, Varela JA (2008) Preparation and characterizations of Ba0.8Ca0.2TiO3 by complex polymerization method (CPM). J Alloys Compounds 465:452-457

Ojamäe L, Aulin C, Pedersen H, Käll P (2006) IR and quantum-chemical studies of carboxylic acid and glycine adsorption on rutile TiO2 nanoparticles. J Colloid Interface Sci 296:71-78

Palmero P, Esnouf C, Montanaro L, Fantozzi G (2005) Influence of the co-precipitation temperature on phase evolution in yttrium-aluminium oxide materials. Journal of the European Ceramic Society 25:1565-1573

Pourbaix M (1974) Atlas of electrochemical equilibria in aqueous solutions. M.Pourbaix, published 1974 by NACE, 644

Qiu H, Gao L, Feng C, Guo J, Yan D (1995) Preparation and characterization of nanoscale Y-TZP powder by heterogeneous azeotropic distillation. Journal of Materials Science 30:5508-5513

Rajendran M, Rao MS (1994) Formation of BaTiO3 from Citrate Precursor. Journal of Solid State Chemistry 113:239-247

Ramanathan S, Kakade MB, Roy SK, Kutty KK (2003) Processing and characterization of combustion synthesized YAG powders. Ceram Int 29:477-484

Su J, Zhang QL, Gu CJ, Sun DL, Wang ZB, Qiu HL, Wang AH, Yin ST (2005) Preparation and characterization of Y3Al5O12 (YAG) nano-powder by co-precipitation method. Mater Res Bull 40:1279-1285

Tachiwaki T, Yoshinaka M, Hirota K, Ikegami T, Yamaguchi O (2001) Novel synthesis of Y3Al5O12 (YAG) leading to transparent ceramics. Solid State Commun 119:603-606

Tanner PA, Law P, Fu L (2003) Preformed sol-gel synthesis and characterization of lanthanide ion-doped yttria-alumina materials. physica status solidi (a) 199:403-415

Townshend A, Jackwerth E (1989) Precipitation of major constituents for trace preconcentration: potential and problems. Pure Appl Chem 61:1643-1656

Vaqueiro P, Arturo Lopez-quintela M (1998) Synthesis of yttrium aluminium garnet by the citrate gel process. J Mater Chem 8:161-163

Veith M, Mathur S, Kareiva A, Jilavi M, Zimmer M, Huch V (1999) Low temperature synthesis of nanocrystalline Y3Al5O12 (YAG) and Ce-doped Y3Al5O12via different sol–gel methods. J.Mater.Chem. 9:3069-3079

Vrolijk JWGA, Willems JWMM, Metselaar R (1990) Coprecipitation of yttrium and aluminium hydroxide for preparation of yttrium aluminium garnet. Journal of the European Ceramic Society 6:47-51

Wang H, Xu X, Zhang J, Li C (2010) A Cost-Effective Co-precipitation Method for Synthesizing Indium Tin Oxide Nanoparticles without Chlorine Contamination. Journal of Materials Science & Technology 26:1037-1040

Wang H, Gao L, Niihara K (2000) Synthesis of nanoscaled yttrium aluminum garnet powder by the co-precipitation method. Materials Science and Engineering: A 288:1-4

Wang L, Zhang L, Fan Y, Luo J, Zhang P, An L (2006) Synthesis of Nd/Si Codoped YAG Powders via a Solvothermal Method. J Am Ceram Soc 89:3570-3572

Xia G, Zhou S, Zhang J, Xu J (2005) Structural and optical properties of YAG:Ce3+ phosphors by sol–gel combustion method. J Cryst Growth 279:357-362

Yang L, Lu T, Xu H, Zhang W, Ma B (2010) A study on the effect factors of sol-gel synthesis of yttrium aluminum garnet nanopowders. J Appl Phys 107:064903

Figure 1a Flow chart of sol-gel process
Click here to download high resolution image

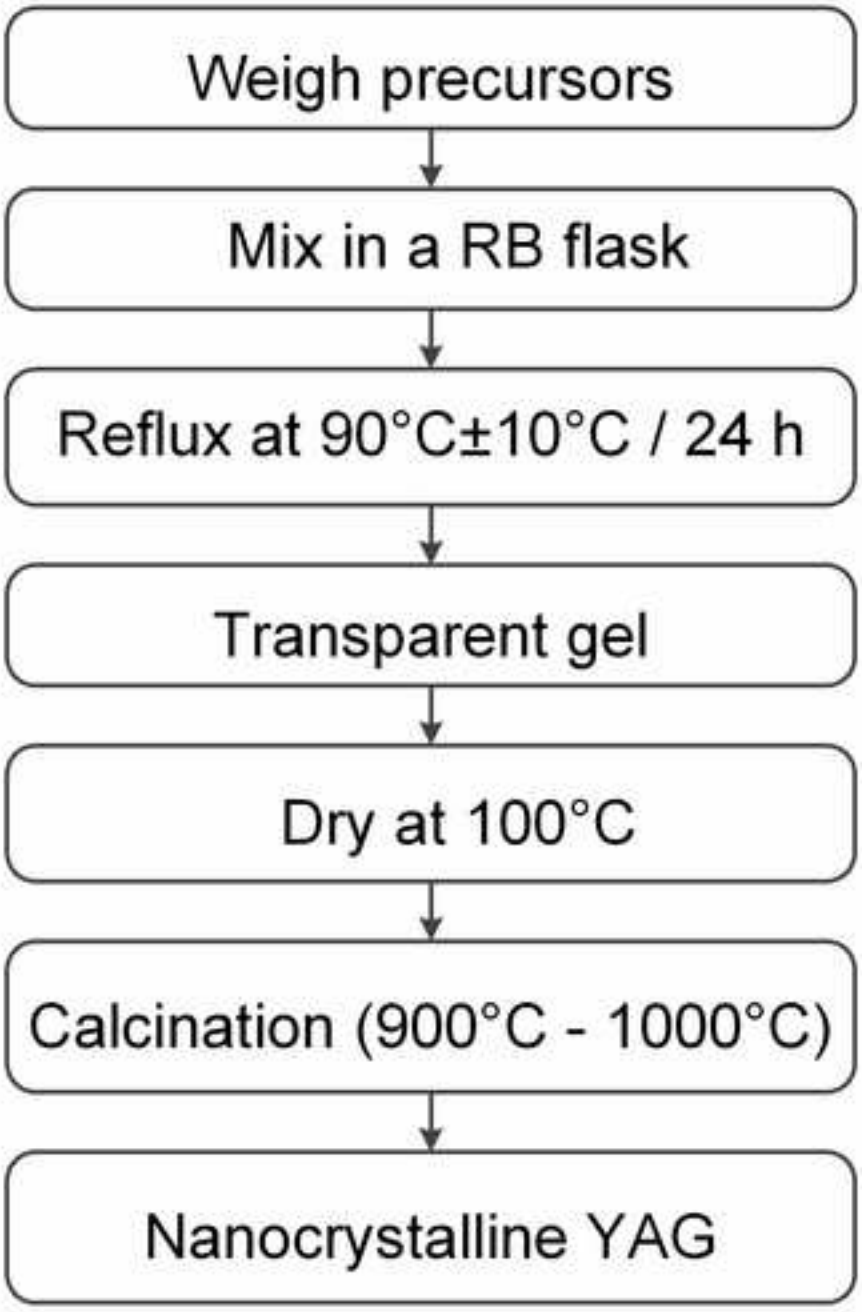

(1 a)

Figure 1b Flow chart of co-precipitaiton process
Click here to download high resolution image

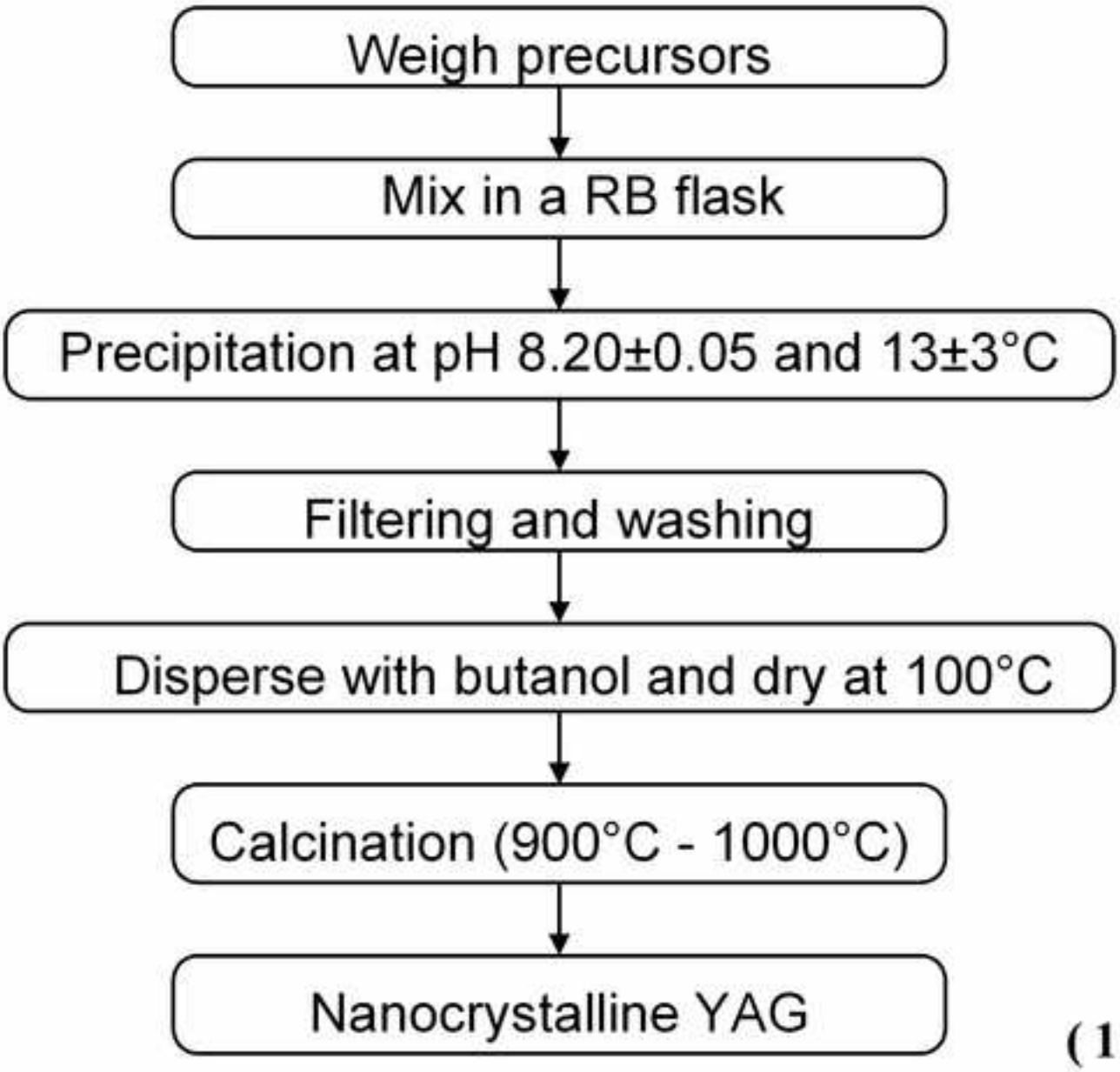

(1 b)

Figure 2a TGA/DSC of SG-YAG powders
Click here to download high resolution image

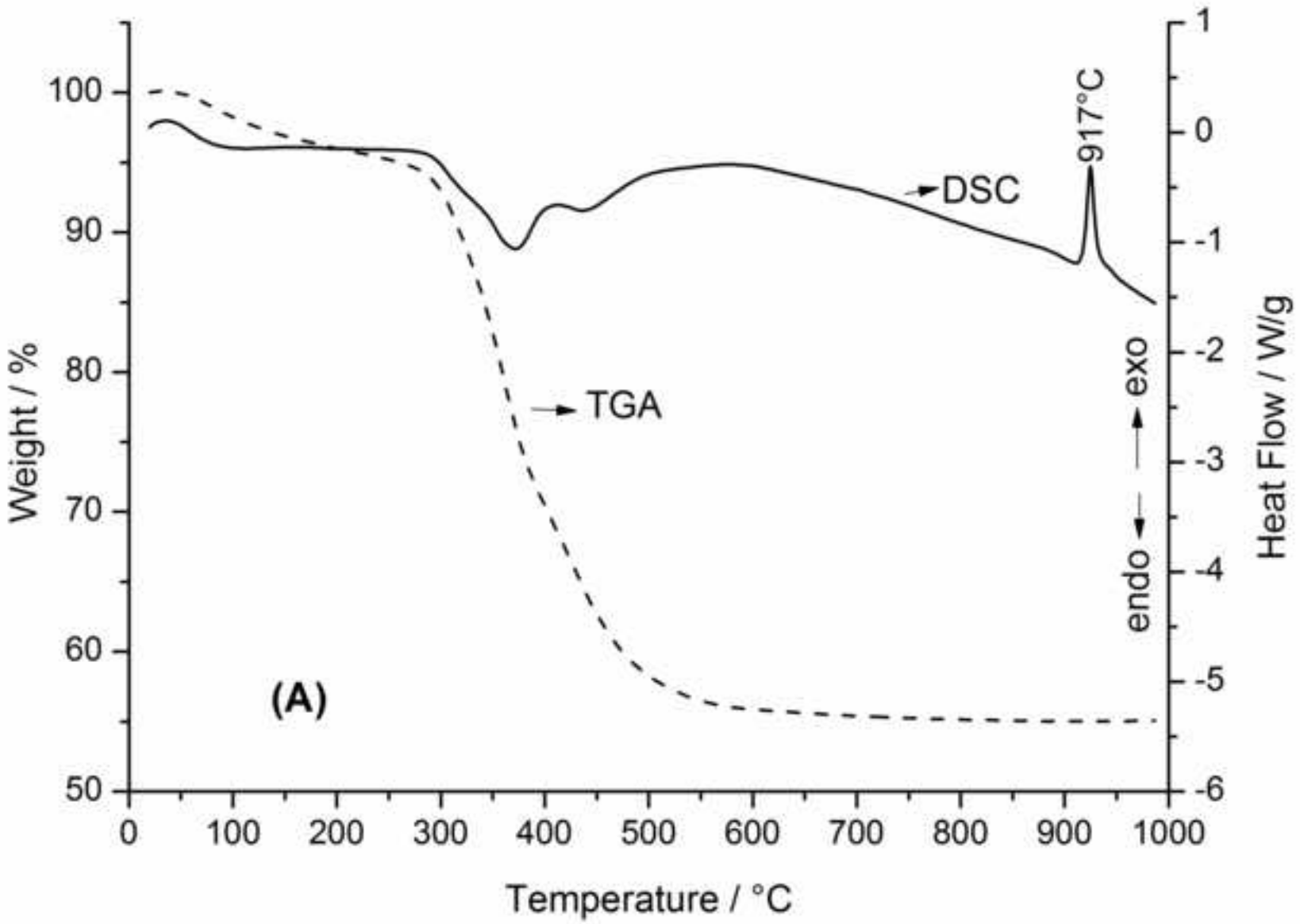

Figure 2b TGA/DSC of CP-YAG powders
Click here to download high resolution image

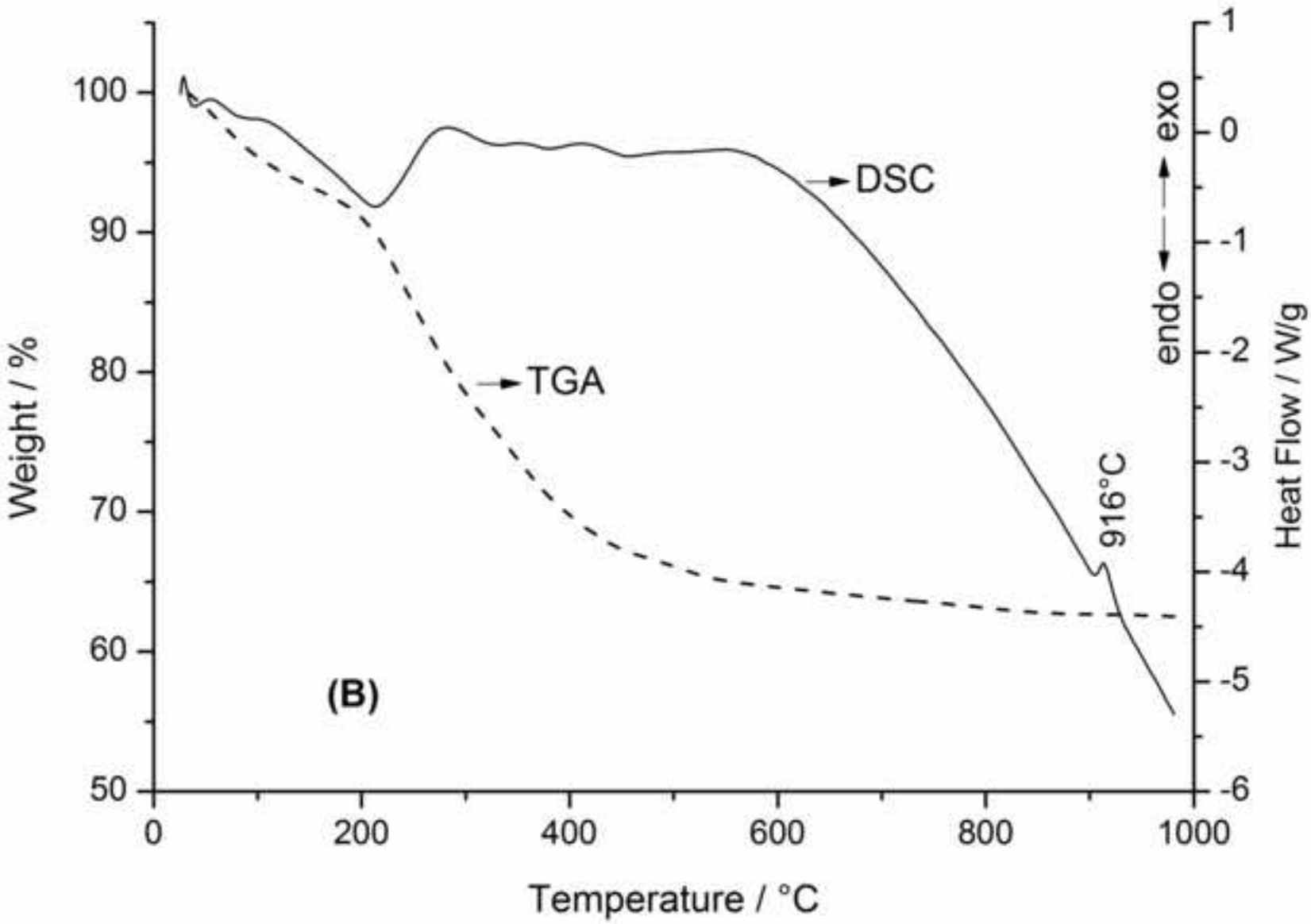

Figure 3a FT-IR spectra of SG-YAG powders
Click here to download high resolution image

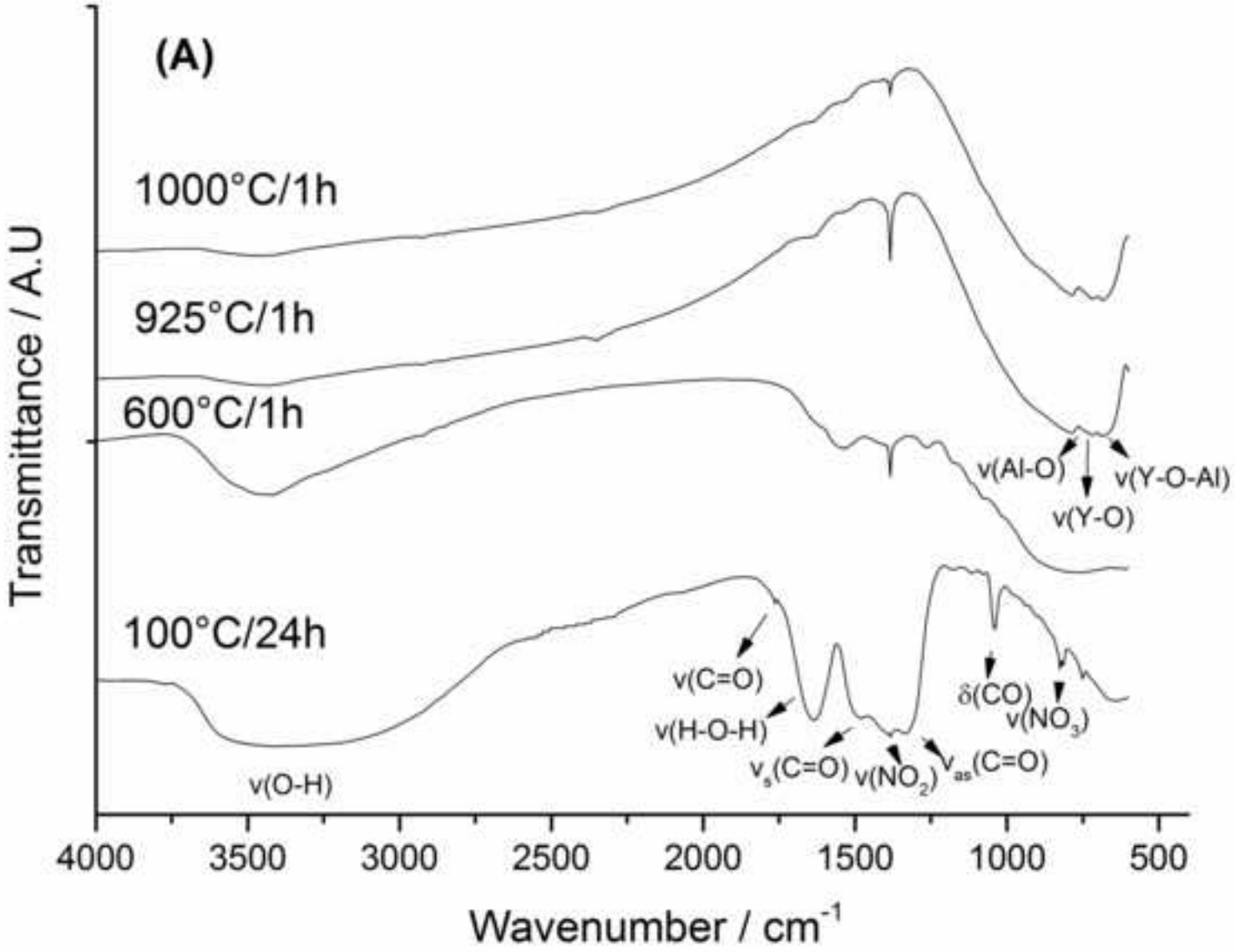

Figure 3b FT-IR spectra of CP-YAG powders
Click here to download high resolution image

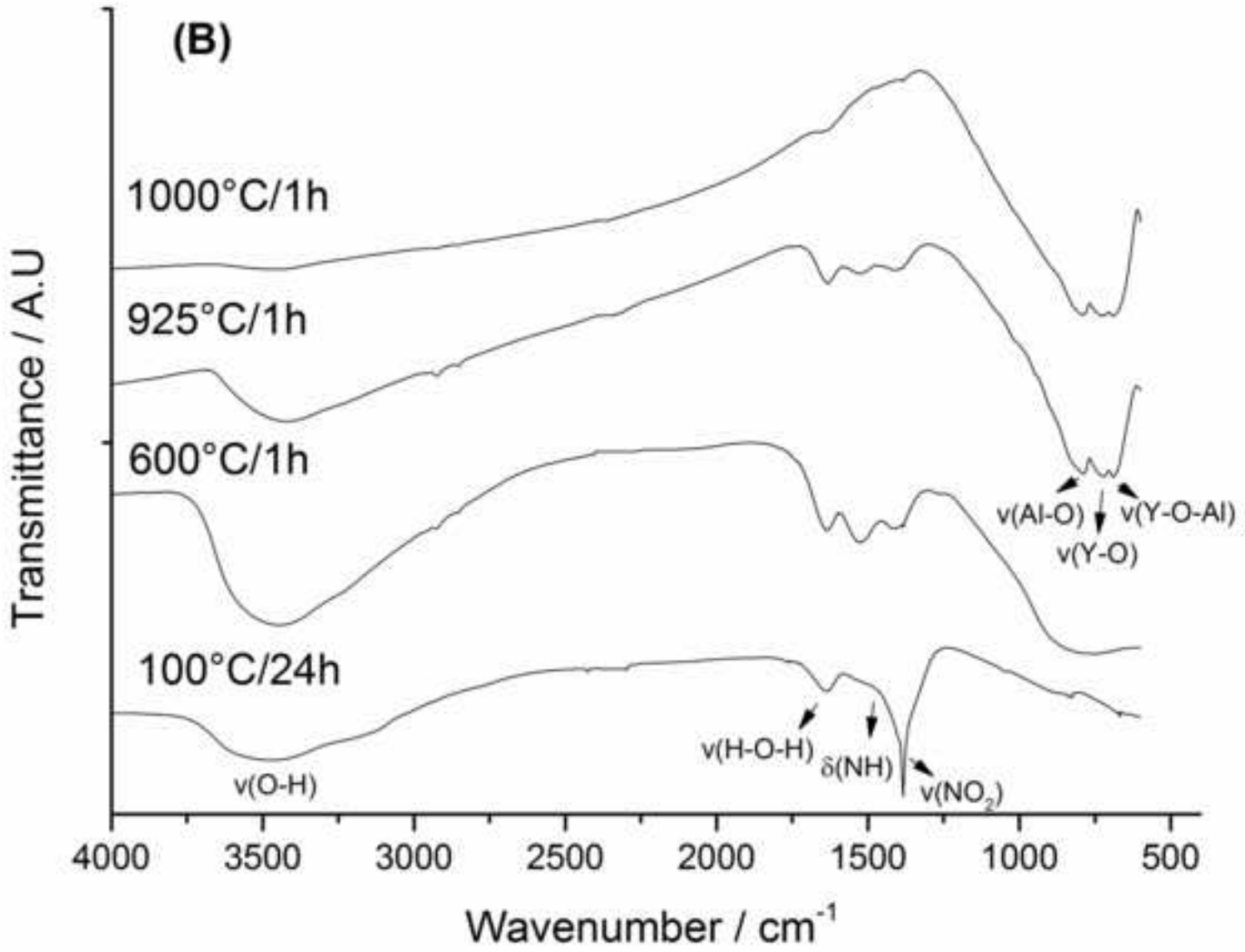

Figure 4a XRD patterns of SG-YAG powders
Click here to download high resolution image

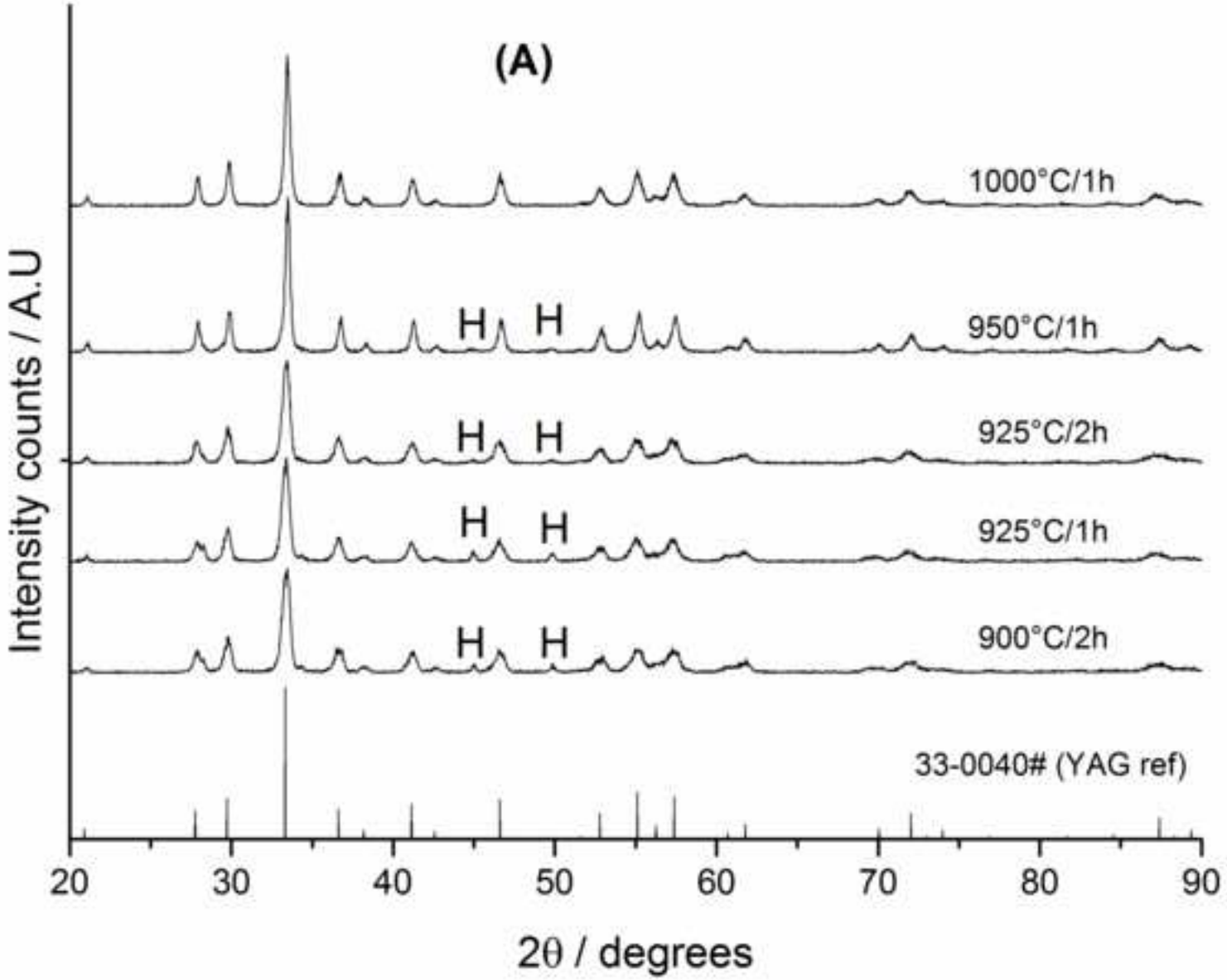

Figure 4b XRD patterns of CP-YAG powders
Click here to download high resolution image

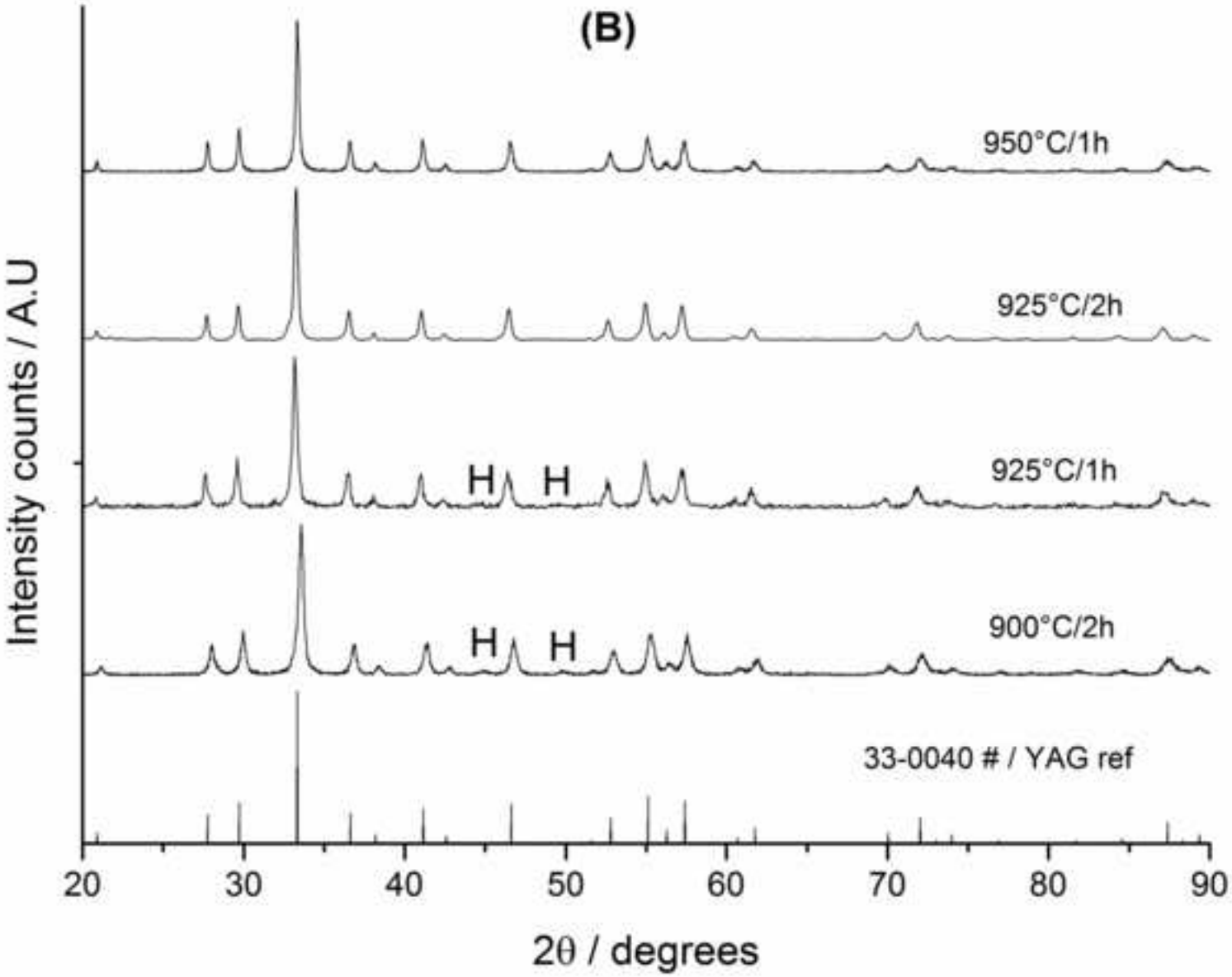

Figure 5a TEM image of SG-nYAG (1000°C), low magnification
Click here to download high resolution image

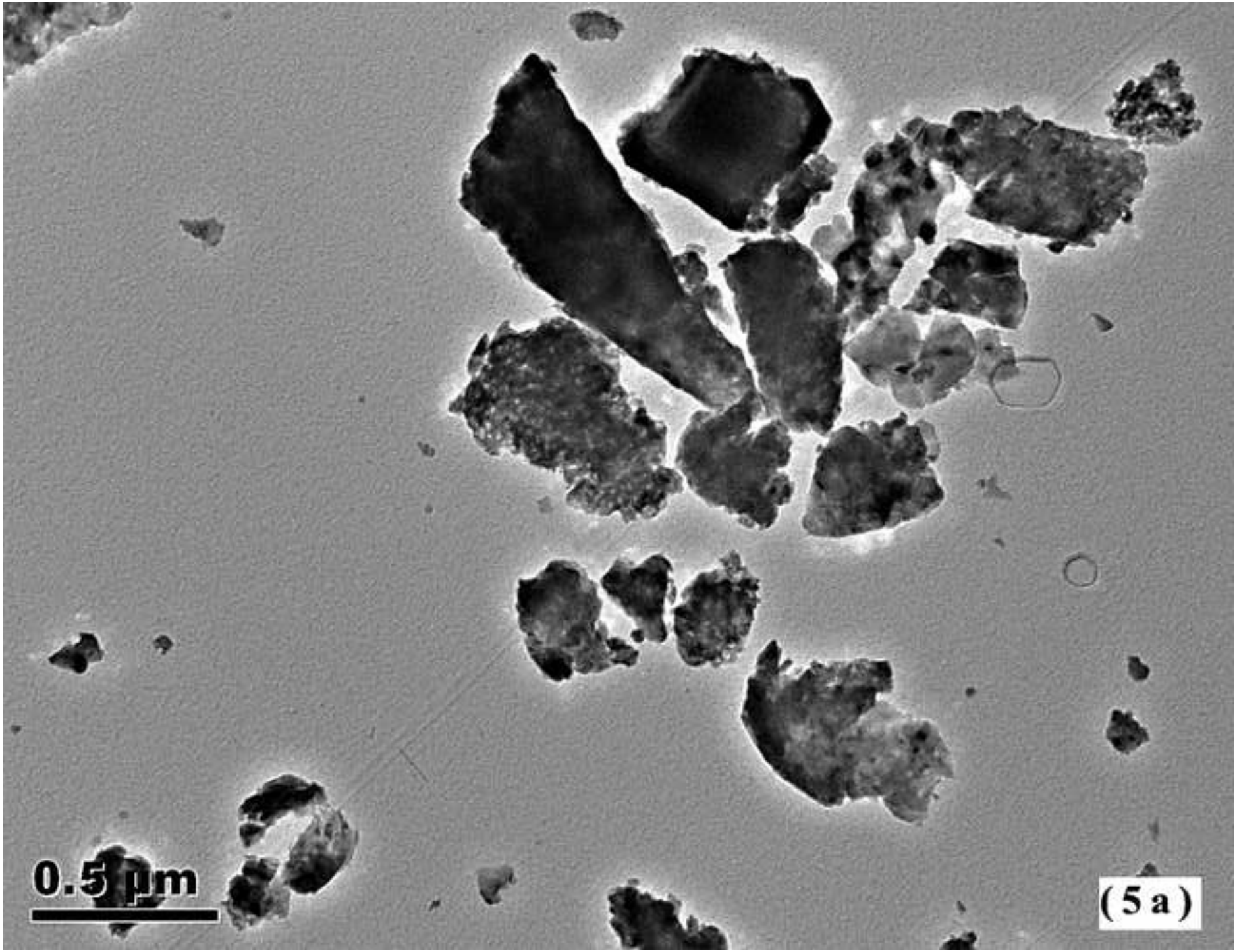

Figure 5b TEM image of SG-nYAG (1000°C), high magnification
Click here to download high resolution image

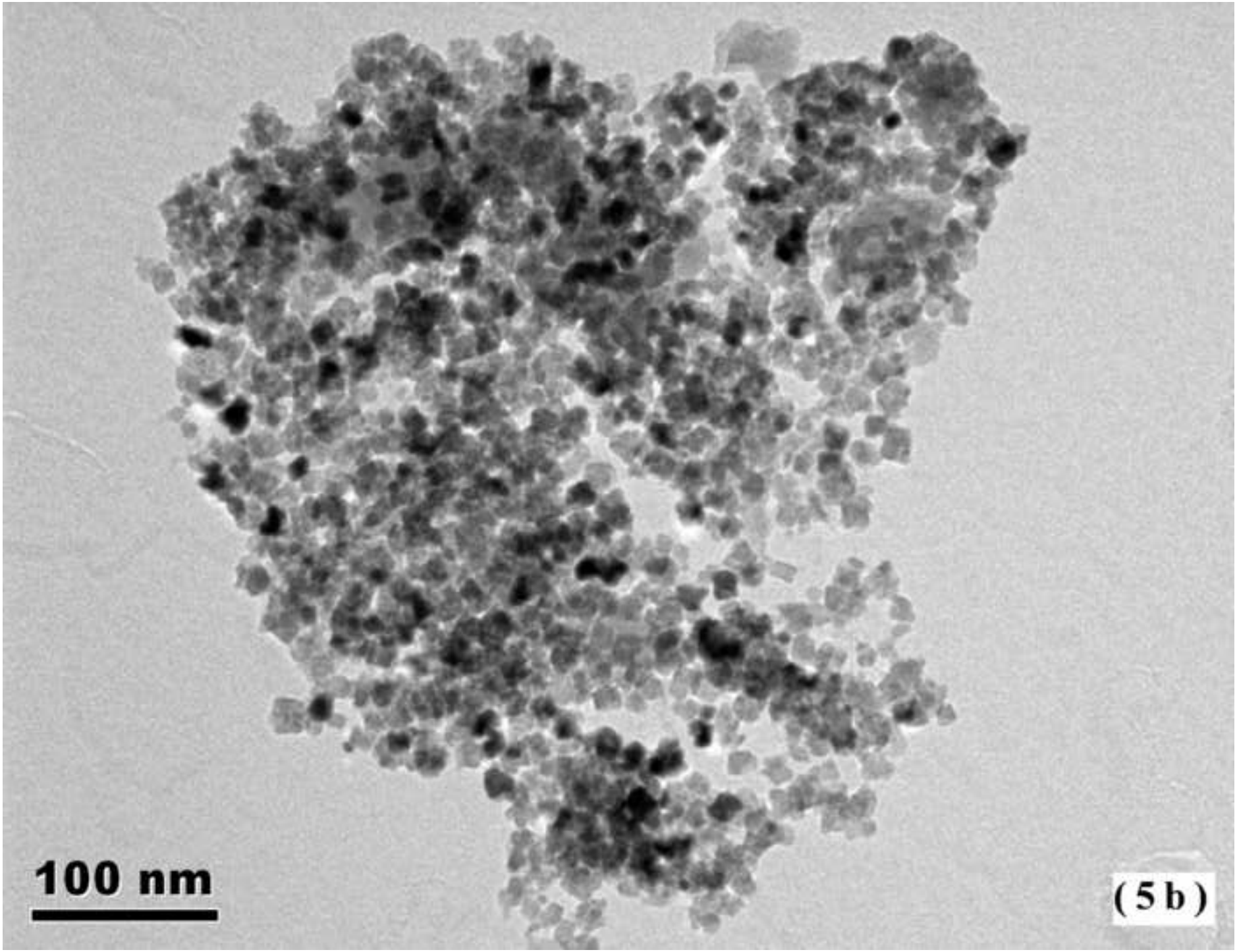

Figure 5c TEM image of CP-nYAG (925°C), low magnification
Click here to download high resolution image

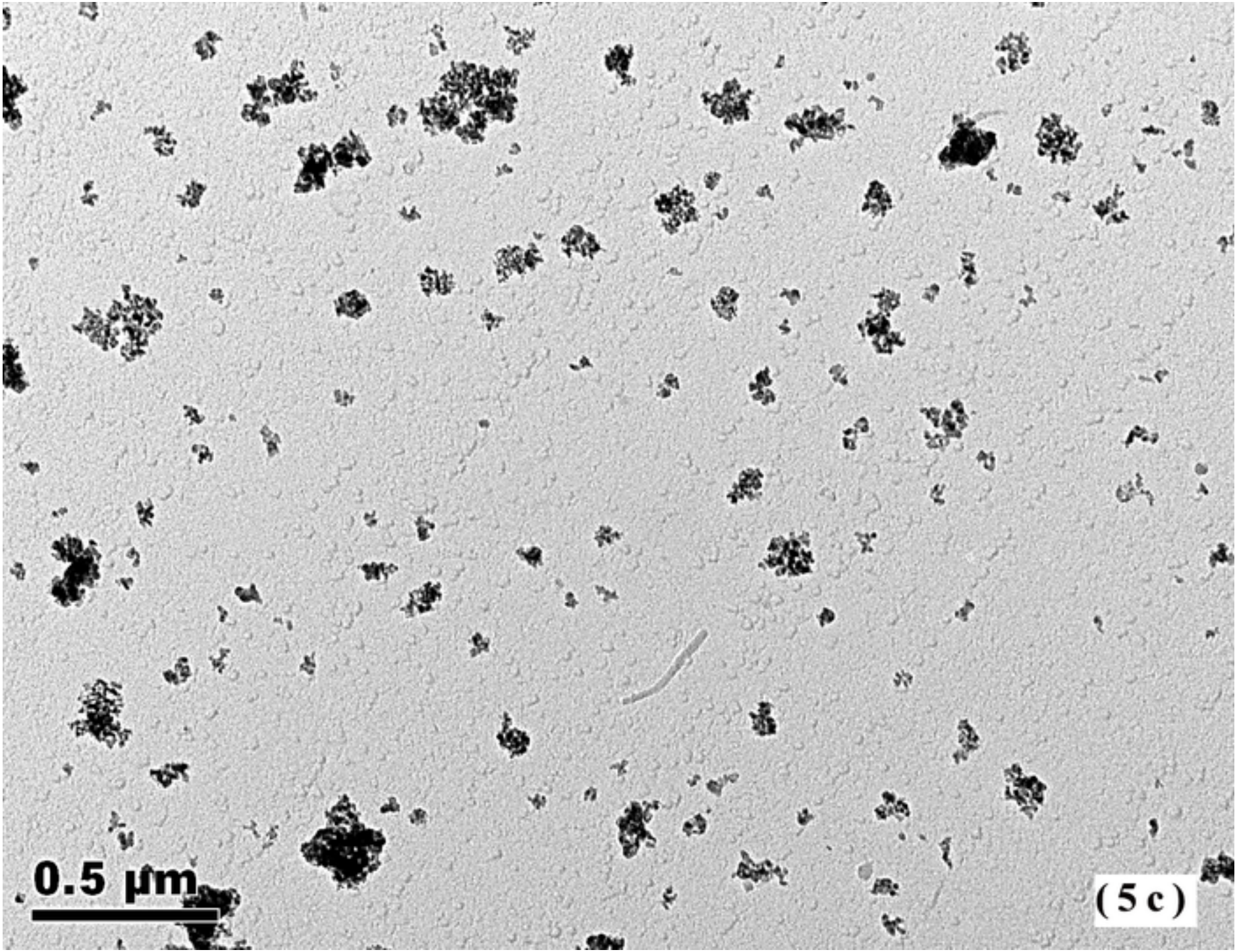

Figure 5d TEM image of CP-nYAG (925°C), high magnification
Click here to download high resolution image

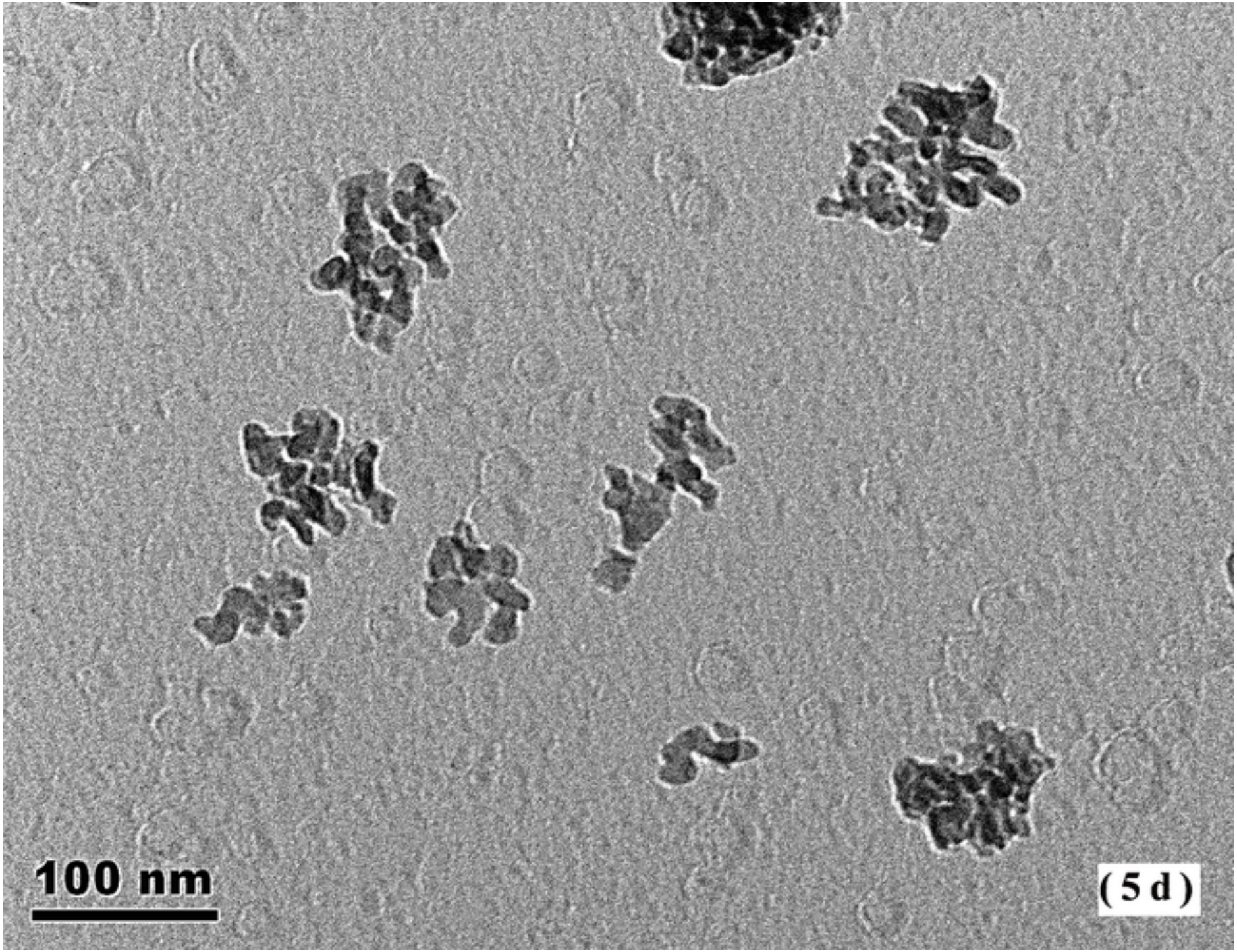

Figure 6a TEM image of CP-nYAG precipitates, 8.10±0.05
Click here to download high resolution image

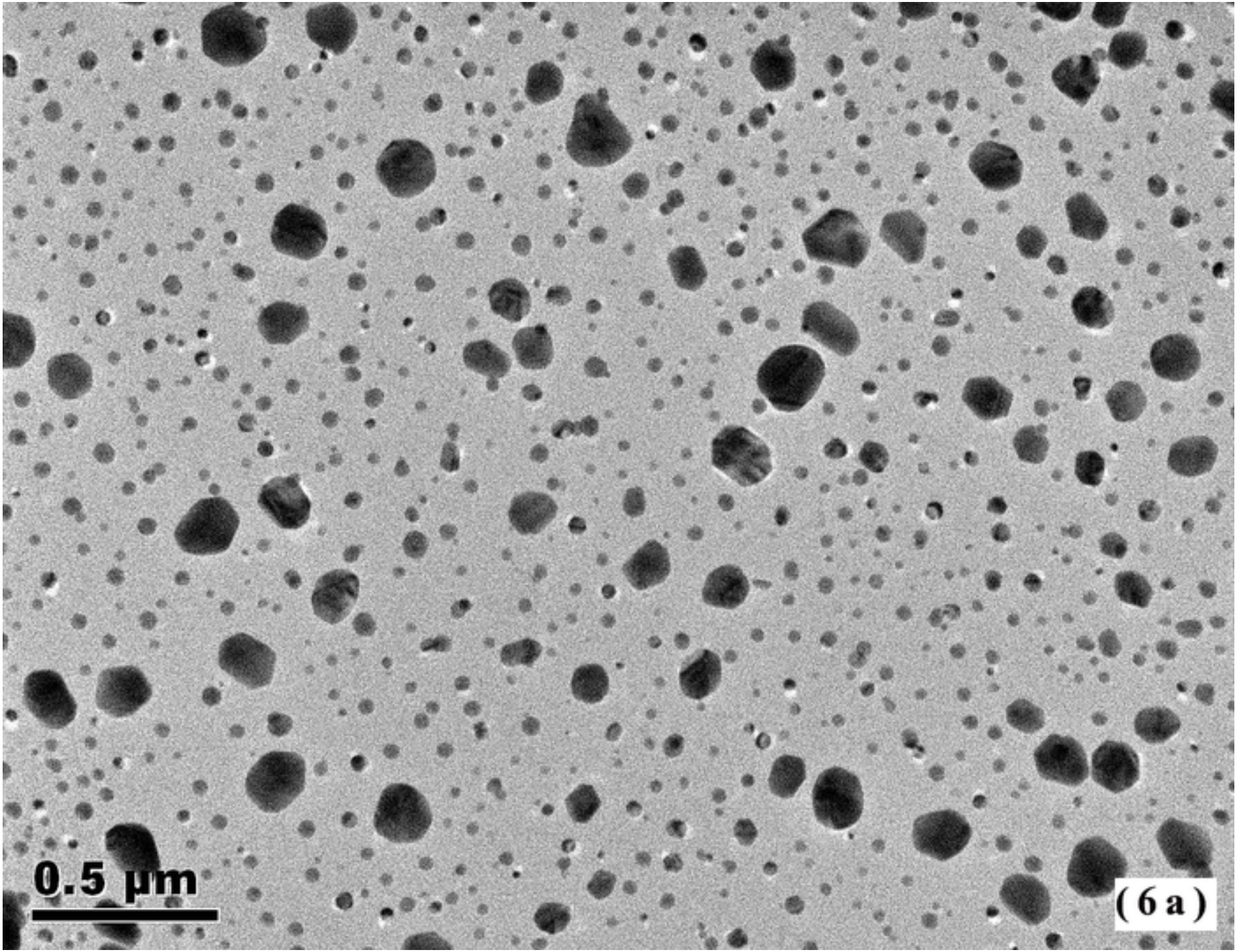

Figure 6b TEM image of CP-nYAG precipitates, 8.20±0.05
Click here to download high resolution image

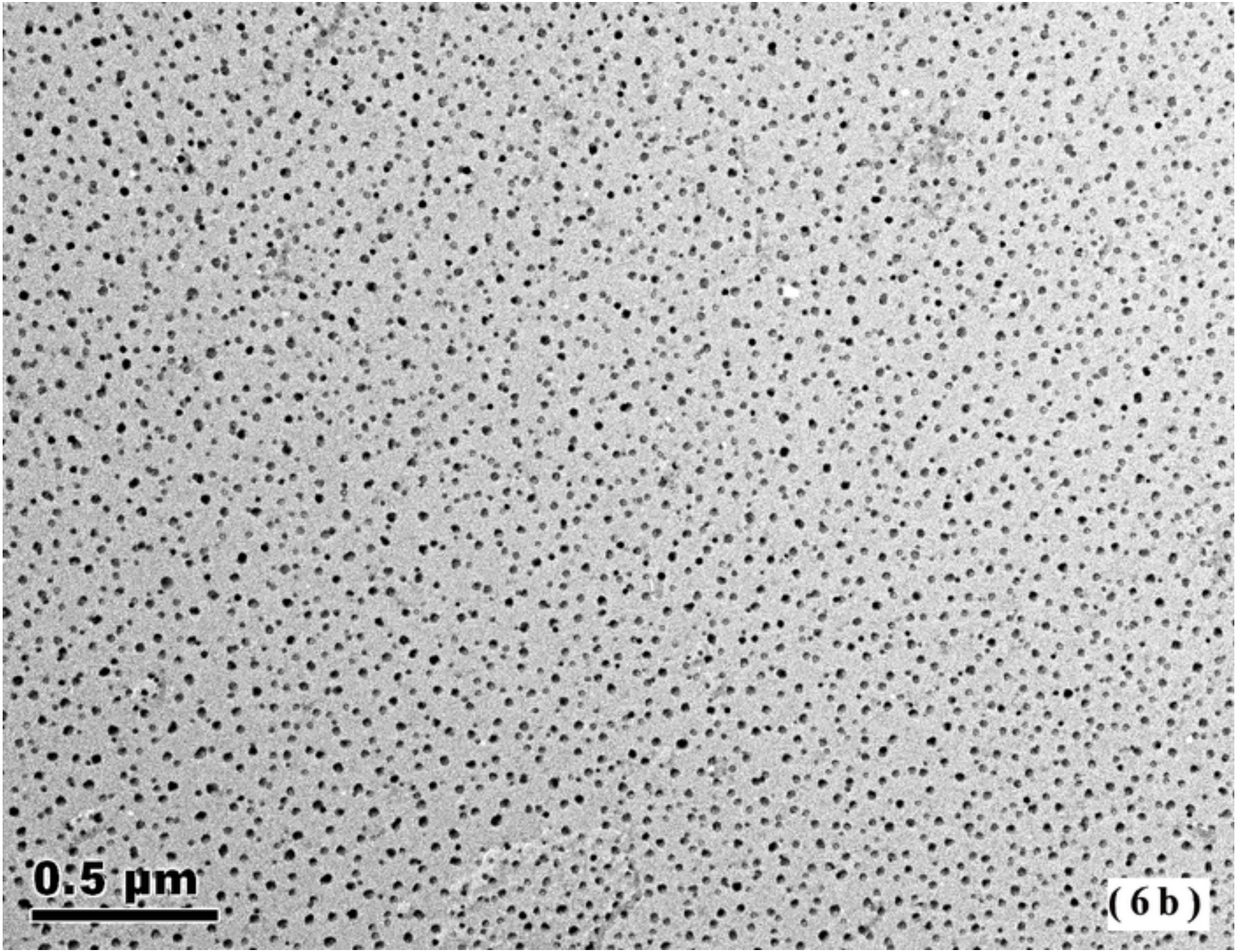

Figure 6c TEM image of CP-nYAG precipitates, 8.30±0.05
Click here to download high resolution image

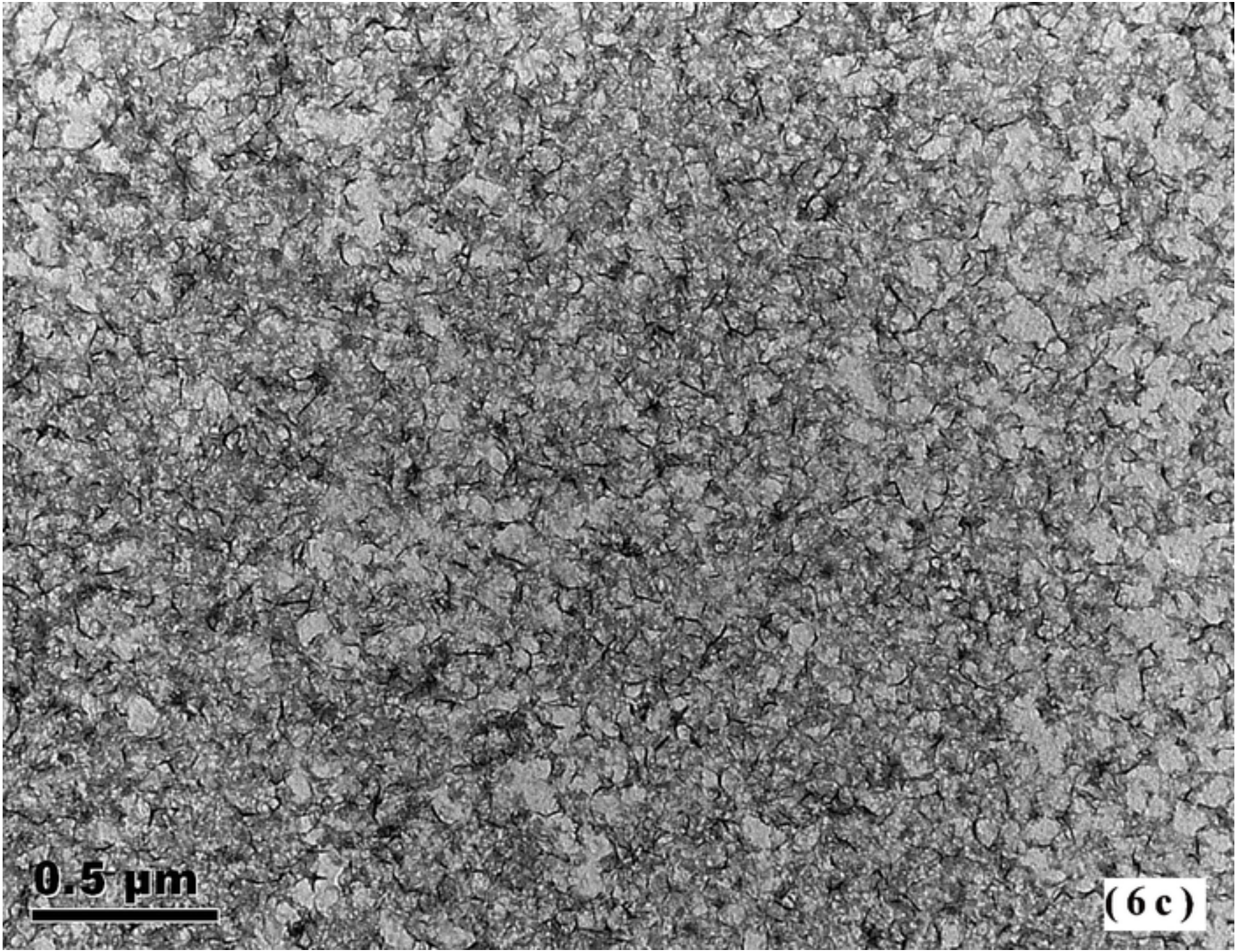

Fig 7 Core/shell image of CP-YAG precipitates, insert: schematic
Click here to download high resolution image

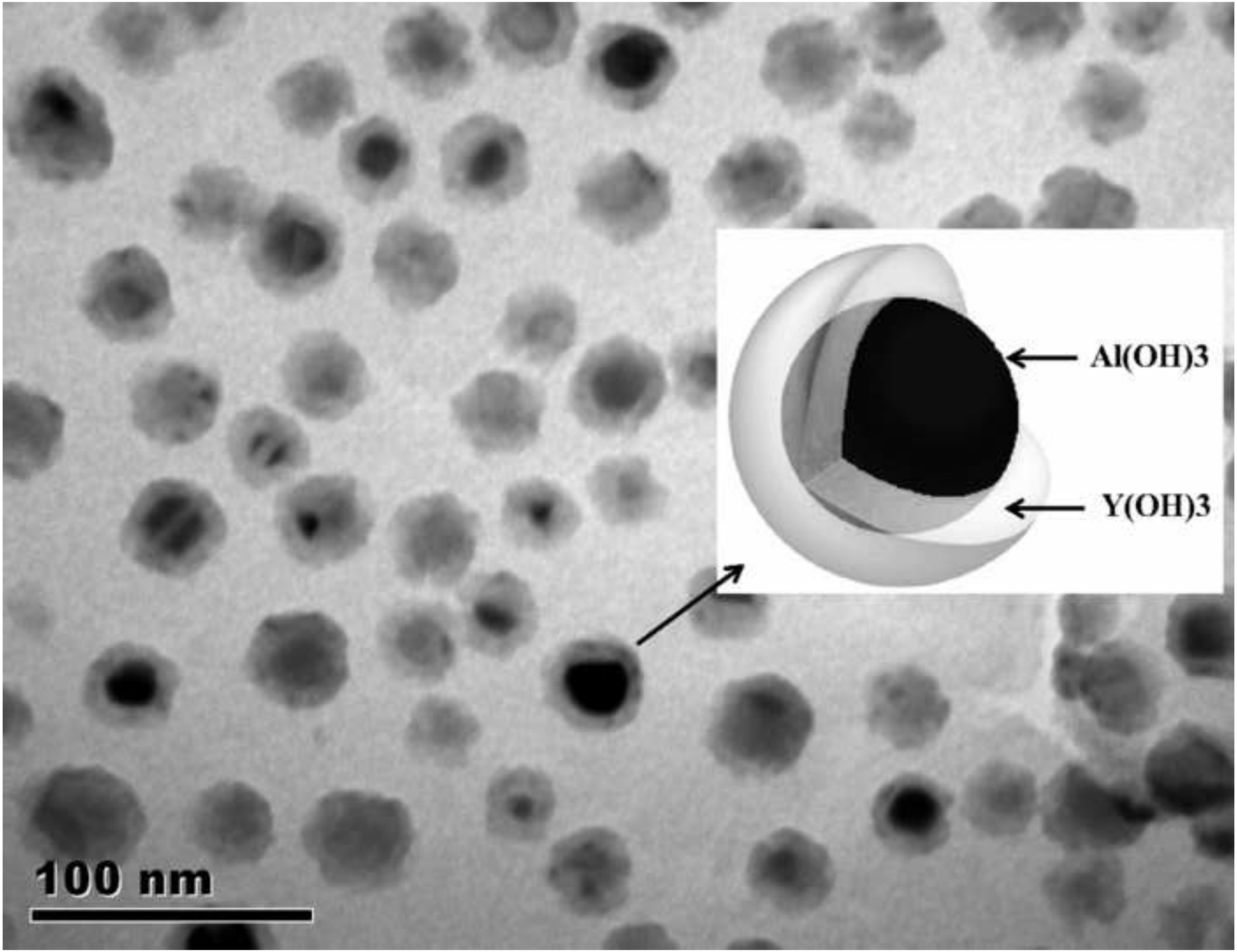

Fig 8a TEM image of CP-YAG precipitates, 10±1°C
Click here to download high resolution image

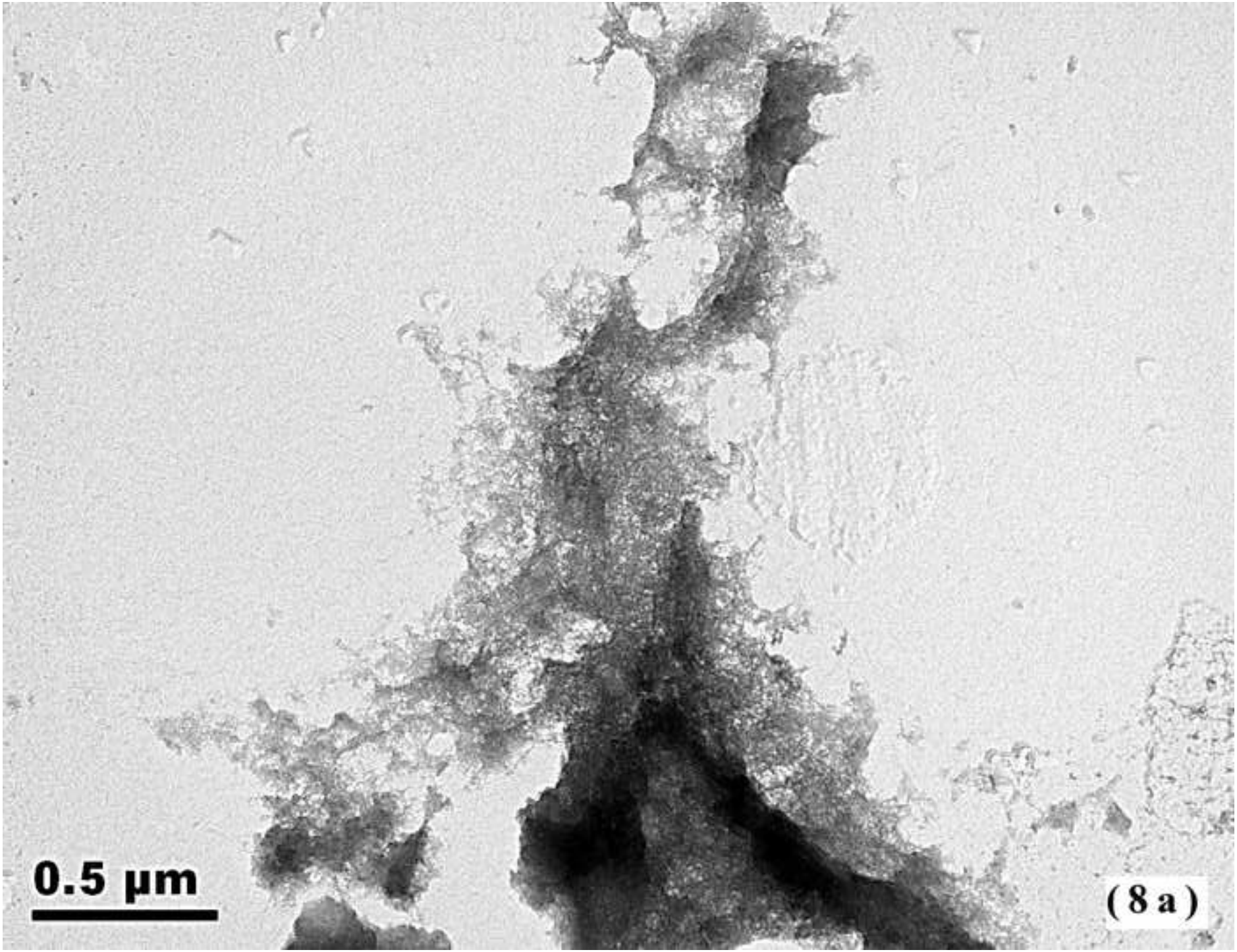

Fig 8b TEM image of CP-YAG precipitates, 13±3°C
Click here to download high resolution image

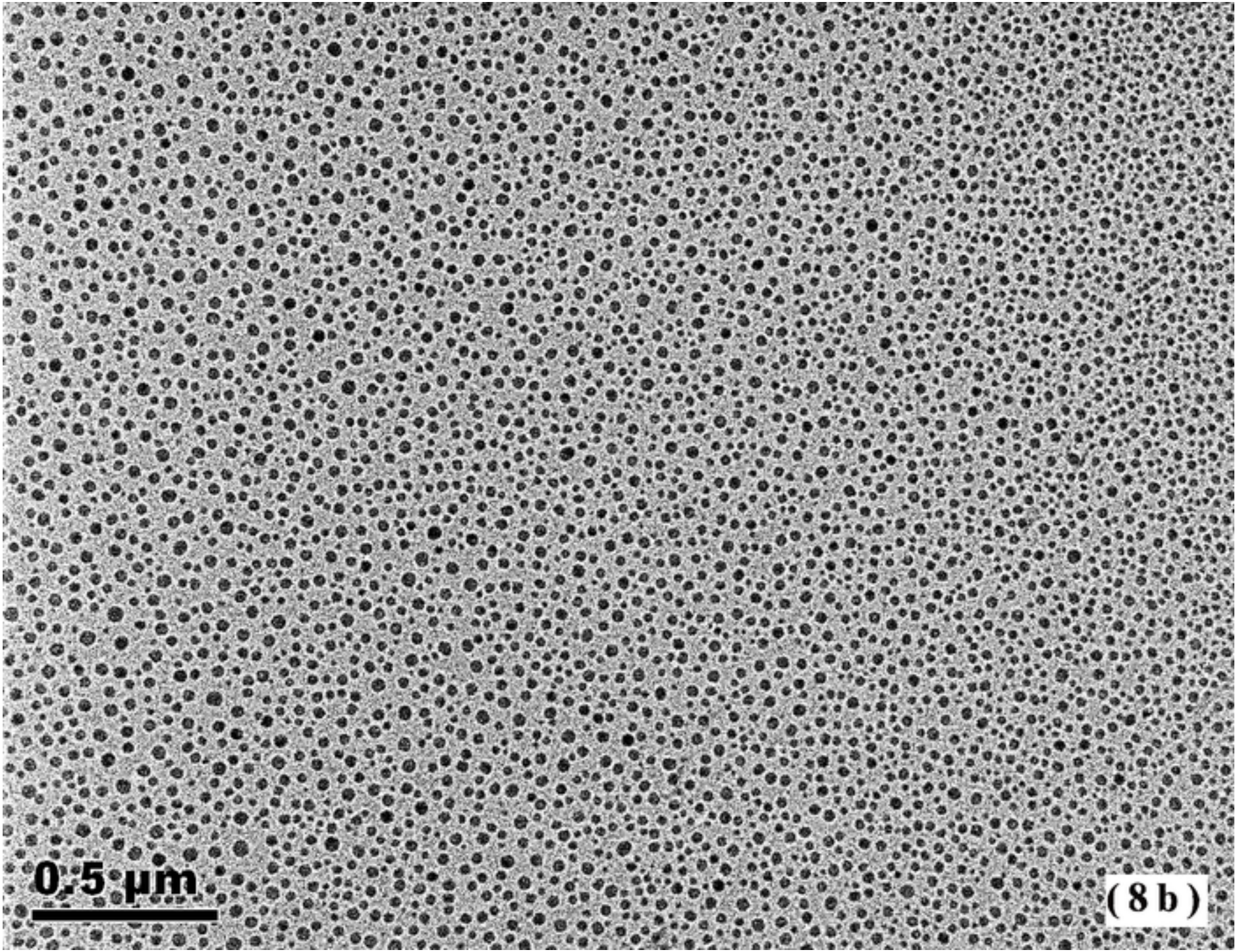

Fig 8c TEM image of CP-YAG precipitates, 20±1°C
Click here to download high resolution image